Bulletin of the Seismological Society of America, 89, 5, pp. 1366–1378, October 1999

Phase Cross-Correlations: Design, Comparisons, and Applications

by Martin Schimmel

Abstract We present a new coherence functional to evaluate quantitatively the goodness of waveform fit between two time series as function of lag time. The proposed coherence measure is called phase cross-correlation (PCC) because it is based on the similarity of instantaneous phases. No amplitudes are explicitly involved, and PCC is therefore an amplitude unbiased measure, which equally weights every sample in the correlation window. As consequence PCC enables to discriminate between closely similar waveforms and is suited to detect weak arrivals that are concealed in larger amplitude signals. Besides, for signal recognition PCC can be applied for arrival time picking, as a misfit function, or it can be used in combination with stacking techniques. The performance of PCC is illustrated and discussed in comparison with the conventional cross-correlation normalized with the geometric mean energy. Both measures are based on different concepts, and the differences in their performance can be significant. The choice of the proper coherence measure depends on the data and application. We show in a data example the ability of PCC to detect weak *P*-to-*s* conversions in the *P*-wave coda of teleseismic events. With this example we give confirming evidence for a crust that is thicker than the global average and for the existence of the 410-km and 660-km discontinuities underneath SE Brazil. In addition, we observe hints of a 510-km discontinuity.

Introduction and Motivation

An important problem in seismology is the unambiguous detection of seismic arrivals to constrain the corresponding Earth structure. Often, difficulties arise because of the variability and abundance of signals in the seismograms. The large amplitude signals are mostly caused by the gross structure of the Earth and although these signals vary in shape, they can be detected due to their outstanding amplitudes. Weak signals, however, are mostly concealed in other signals with similar amplitudes. As a consequence, the weak signals can only be detected because of their coherent appearance on different seismograms or their resemblance with a given reference or pilot wavelet such as the direct *P* arrival or the imposed ground signal of a vibrating source. The detection, arrival time picking, and/or extraction of weak signals therefore require the use of coherence measures. Because the weak signals are more sensitive to waveform perturbations than the large amplitude signals, the problem consists in the detection of closely similar waveforms rather than completely coherent waveforms. To cope with this problem, a variety of coherence measures have been innovated to evaluate quantitatively the goodness of fit obtained. These measures are mostly based on cross-correlation and stacking techniques which are used widely at various stages of data processing.

The cross-correlation between two data sets measures their similarity as a function of time shift or time lag. This measure involves the progressive sliding of one waveform past the other and the summation of the cross-multiplication products over the common time interval of the waveforms. The cross-correlation function will be peaked at time lags when the (closely) similar waveforms are best aligned. Dissimilar waveforms cause the cross-correlation function to have small amplitudes due to the summation of positive and negative cross-multiplication products. Various cross-correlation techniques have been designed (e.g., Neidell and Taner, 1971; Gelchinsky *et al.*, 1985). These methods are mostly used in combination with stacking techniques and are, for instance, applied to determine the optimal stacking velocities in seismic exploration. VanDecar and Crosson (1990) constructed a semi-automated approach for arrival time picking in multi-channel data. They efficiently cross-correlate all possible pairs of traces and solve for the relative arrival times using least-square criteria. Cross-correlations have also been used to design different fitness or objective functions in waveform inversions (Sen and Stoffa, 1991; Diogo, 1995).

In principle, stacking techniques can be employed whenever the signals on the different traces have similar shape. The average signal is expected to be enhanced by constructive summation along the correct travel time curve while the surrounding uncorrelated noise decreases. Difficulties in suppressing noise with ordinary stacks might occur

when the signals are weak and when the amount of data is small. This led to nonlinear stacking techniques like the *n-th*-root stack (Muirhead, 1968; Kanasewich *et al.,* 1973) and the phase-weighted stack (Schimmel and Paulssen, 1997). A number of other stacking techniques exists. Inverse theory has been applied by Neele and Snieder (1991) to increase the resolution of conventional beamforming for array data. Mao and Gubbins (1995) simultaneously solve for delay times and stacking weights by minimizing waveform fits between each trace and the beam of the weighted remaining traces. Krüger *et al.* (1993) combine source- and receiver array beamforming to a double beam technique. Coherent harmonic signals, such as the eigenmodes of the Earth, can be detected on single time series with the phasor-walkout method (Zürn and Rydelek, 1994). This method is based on phase-coherence, which nicely reveals the random, coherent, or periodic nature of signals in a complex spectrum. The same principles of phase-coherence have been employed by Schimmel and Paulssen (1997) to design the phase stack, which is an amplitude unbiased coherence measure.

Here we extend the concept of the phase stack and present a new cross-correlation function that we call phase cross-correlation (PCC). The proposed function can be used as a coherence function and for signal recognition and arrival-time picking. We show synthetic applications, which are discussed in comparison with the conventional cross-correlation and the geometric normalized cross-correlation. It is shown that the geometric normalized cross-correlations and phase cross-correlations of closely similar waveforms can lead to different results due to their different design philosophies. The geometrical normalized cross-correlation is insensitive to the amplitude changes between data sets but is biased by the large amplitude portions within the considered correlation windows. Conversely, PCC equally weights every sample in the correlation and is consequently insensitive to the amplitudes within the correlation windows.

Finally, we apply the normalized cross-correlation and PCC to a data set of Brazilian seismic broadband recordings to detect weak upper mantle *P*-to-*s* reflections/conversions underneath SE Brazil. The results and performance of the correlations are compared and briefly discussed with respect to the seismic visibility of upper mantle discontinuities. Here we are more interested in the technical aspects of signal recognition rather than the structural implications of the observed phases.

The Method

We design a cross-correlation method for signal recognition and arrival-time picking. The result, PCC, represents an amplitude unbiased coherence measure of wavelets. This method of PCC employs complex trace analysis and is based on the similarity of the instantaneous phases of the analytic traces. The PCC method is an extension of the phase stack technique presented by Schimmel and Paulssen (1997). First, we briefly summarize the principles of the phase stack and then we explain PCC using these principles.

Design of the Phase Cross-Correlation

The phase stack is an amplitude-unbiased coherence measure that is based on complex trace analysis. Therein a complex trace or analytic signal $S(t)$ is constructed by ascribing the real seismic trace $s(t)$ to the real part of $S(t)$ and its Hilbert transform $H[s(t)]$ to the imaginary part of $S(t)$. The analytic signal is thus uniquely determined by the seismic trace $s(t)$. The $S(t)$ is often expressed with time-dependent amplitude $A(t)$ and phase $\phi(t)$:

$$S(t) = s(t) + iH[s(t)] = A(t)e^{i\phi(t)}. \tag{1}$$

$A(t)$ and $\phi(t)$ are also called the envelope and instantaneous phase, respectively (e.g. Bracewell, 1965). The analytic signal $S(t)$ can be visualized as a vector with length $A(t)$ that rotates with increasing time in the complex space around a time axis (Taner *et al.* 1979). In this visualization the seismic trace is the projection of this helix-like curve onto the surface spanned by the real axis and the time axis.

The phase stack $c_{ps}(t)$ (equation 2) is obtained by the sum of N normalized analytic traces.

$$c_{PS}(t) = \frac{1}{N}\left|\sum_{j=1}^{N} e^{i\phi_j(t)}\right| \tag{2}$$

This measure is amplitude-unbiased because no amplitudes are explicitly involved. Because of the complex summation, $c_{ps}(t)$ employs the principles of constructive and destructive interference. The amplitudes of the phase stack range between 0 and 1 as function of time. Amplitude 1 is achieved when the signals are perfectly phase-coherent. Zero amplitude means that the signals summated completely destructively. Here we apply these principles to design a cross-correlation, which we call PCC in analogy to the phase stack.

The objective is to detect the signals in a seismic trace $s_1(t)$ that are coherent with a reference or pilot wavelet $s_2(t)$. For this purpose wavelet $s_2(t)$ is shifted in time and compared with the corresponding portion on the seismic trace $s_1(t)$. We employ the phase stack as coherence measure to determine the similarity at every time sample. This is easily performed by the following summation:

$$c(t) = \frac{1}{2N}\sum_{\tau=\tau_0}^{\tau_0+T} |e^{i\phi(t+\tau)} + e^{i\psi(\tau)}|, \tag{3}$$

$e^{i\phi(t)}$ and $e^{i\psi(t)}$ are the amplitude-normalized analytic signals of the seismic trace $s_1(t)$ and the wavelet $s_2(t)$. At time t the phase stack is calculated at each time sample τ for the length T of the pilot wavelet. All N samples of the phase stack are added to obtain one number, which measures the similarity at time lag t. The normalization $1/(2N)$ ensures that this number becomes 1 in the case of the complete coherence of both

data sets. In the case that the signals are anticorrelated, that is, when the signals are coherent but have different polarity, $c(t)$ becomes 0. This is in fact not what we want: 0 amplitude should be assigned when there is no coherency at all, and an amplitude of 1 should be assigned when the signals are anticorrelated. Consequently, we extend equation (3) with a modified phase stack, which similarly determines the anticorrelation of the signals. The result is shown in equation (4) and presents the PCC measure.

$$c_{\mathrm{PCC}}(t) = \frac{1}{2N} \sum_{\tau=\tau_0}^{\tau_0+T} \{|e^{i\phi(t+\tau)} + e^{i\phi(\tau)}| - |e^{i\phi(t+\tau)} - e^{i\phi(\tau)}|\} \tag{4}$$

When the signals are perfectly correlated, the last term in the summation becomes 0 at all samples τ. For anticorrelated signals, this term becomes 2 while the first term has 0 amplitude. If there is no correlation, both terms almost equal and subtract to a small number. $c_{pcc}(t)$ measures the coherence between two data sets as function of lag time such as the conventional cross-correlation function does. The amplitudes range between -1 and 1. Equation (4) reduces after the introduction of the cosine and sine functions to equation (5),

$$c_{\mathrm{PCC}}(t) = \frac{1}{N} \sum_{\tau=\tau_0}^{\tau_0+T} \left\{ \left| \cos\left(\frac{\phi(t+\tau) - \psi(\tau)}{2}\right) \right| - \left| \sin\left(\frac{\phi(t+\tau) - \psi(\tau)}{2}\right) \right| \right\}. \tag{5}$$

Application to Synthetic Data

In the following sections we show synthetic applications and discuss the PCC in comparison with the conventional cross-correlation (CC) and the geometric normalized cross-correlation (CCGN). First we consider the detection of coherent signals and then we discuss the coherence and detection of closely similar waveforms.

Comparison with other Cross-Correlation Functions

The cross-correlation is a much used coherency measure between two data sets. It has widely been used for different applications. As consequence, there exists a large number of different coherence measures which are based on the cross-correlation. We use the CC and CCGN. The CCGN is chosen since it is insensitive to amplitude changes between the data sets. This measure varies between -1 and $+1$, where $+1$ corresponds to perfect sign coherency, and -1 corresponds to the perfect coherency of signals of different polarity. The CCGN as function of time of sample t between two traces $s_1(t)$ and $s_2(t)$ has the following form:

$$c_{\mathrm{CCGN}}(t) = \frac{\sum_{\tau=\tau_0}^{\tau_0+T} s_1(t+\tau)s_2(\tau)}{\sqrt{\sum_{\tau=\tau_0}^{\tau_0+T} s_1(t+\tau)^2 \sum_{\tau=\tau_0}^{\tau_0+T} s_2(\tau)^2}}. \tag{6}$$

The summations are performed over a time window of length T. The denominator is the geometric mean of the energy of the two traces within the time window chosen.

Detection of Coherent Signals

We calculate PCCs, CCs and CCGNs between two different test traces and pilot wavelets. The results are compiled in Figure 1a and b. The trace at the top of each figure shows a synthetic time series with four wavelets. The wavelets are labeled with numbers. Wavelet 1 and wavelet 3 have the same waveform as wavelet 2 and wavelet 4, respectively. They differ only in amplitude and polarity. Wavelet 3 is the pilot that is used for the cross-correlations with the synthetic trace. The second, third, and fourth trace (Fig. 1) show the results of the different cross-correlations. From top to bottom these are PCC, CC, and CCGN. The envelopes of the PCC (solid line) and CCGN measure (dashed line) are plotted in the lowest panel. The CCGN measure is not normalized whenever the norm becomes smaller than 5% of the maximum norm. This constraint is implemented to avoid numerical problems due to the zero amplitude sections in the trace. Theoretically, the analytic signal of the zero amplitude sections does not have a phase; however, numerically a phase zero is ascribed to a zero amplitude signal.

From Figure 1 it is obvious that CC is an amplitude-biased coherence measure. Wavelets with similar waveform but different amplitudes have different cross-correlation values. Conversely, PCC and CCGN are not sensitive to the amplitude variations of the phase-coherent wavelets. This is inherent to the concept of PCC and the geometric normalization (denominator in equation 6) of CCGN. Note that the absolute maximum of the CC measure in Figure 1b is obtained for wavelet 1, which is not coherent with the pilot (wavelet 3). This can happen because the conventional cross-correlation is based on the products of the amplitudes, which are the largest for wavelets 1 and 3. It shows the need to normalize the CC.

Figure 1 further shows the ability to detect the similar waveforms (wavelets 3 and 4) with the pilot wavelet using the PCC and CCGN measure. With PCC a better signal-to-noise ratio (SNR) is obtained. The oscillations of the PCC around wavelet 3 and 4 in Figure 1a are due to the narrow-band wavelet and the insensitivity of PCC to the amplitudes of the waveform. The fast decay of amplitudes of wavelet 3 is the reason for the decay of the corresponding oscillation in the CC and CCGN measure, which are based on the multiplication of these amplitudes.

Further examples of PCCs and CCGNs are plotted in Figure 2. Figure 2a shows a random time series and three

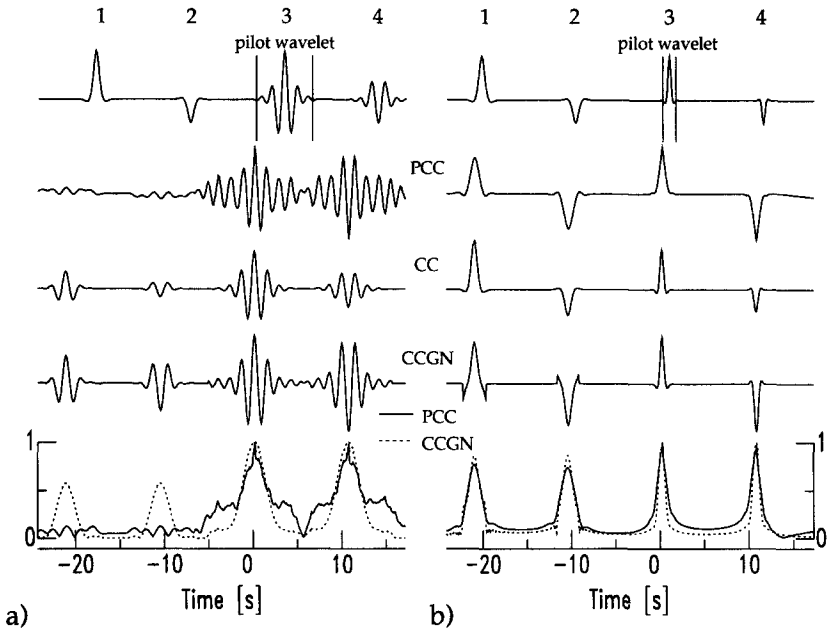

Figure 1. (a) The first trace shows the synthetic time-series and pilot wavelet that are used to compute the cross-correlograms. From top to bottom, these are PCC, CC, and CCGN. In the lower-most panel we compare the envelopes of PCC (solid line) and CCGN (dashed line). (b) Same as (a) but for a different time series and pilot.

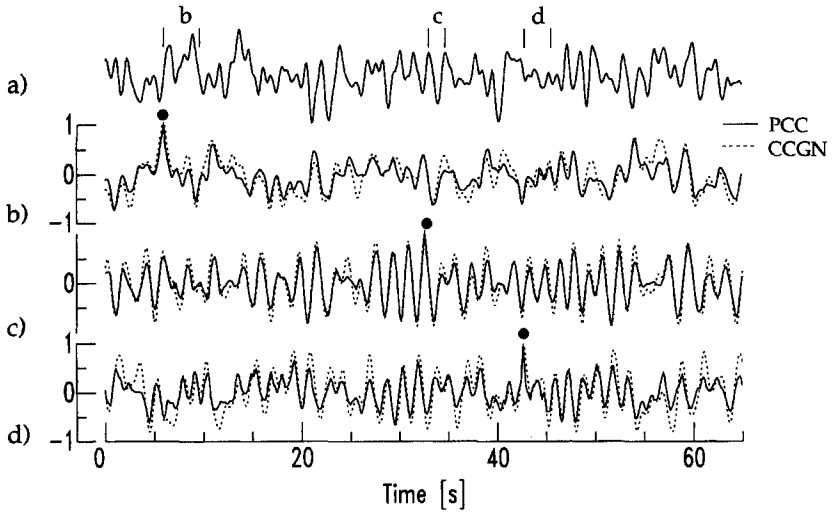

Figure 2. (a) Seismic test trace and three pilot wavelets used to calculate the PCCs and the CCGNs that are shown in Figures b–d. The vertical lines mark the begin and end times of the employed pilots. We use the labels b,c, and d to refer to these wavelets. (b) PCC (solid line) and CCGN (dotted line) between wavelet b and test trace. (c) Same as (b) but wavelet c is used. (d) Same as (b) but wavelet d is used.

arbitrarily selected pilots. We label these wavelets b, c, and d. The begin and end times of these wavelets are marked by the vertical lines. Wavelet b and d look complicated and are distinct from the rest of the trace. Conversely, wavelet c is not recognizably different from other portions of the time series. Figures 2b, c, and d show the PCCs (solid lines) and CCGNs (dashed lines) between the wavelets b, c, and d, and the trace from Figure 2a. The black dots mark the absolute maxima of the cross-correlograms that are located at the beginning of the pilot wavelets. They mark what we call signal in this example. As can been seen in Figure 2, the SNR of the different cross-correlograms depends on the waveform complexity of the pilot waveform. Note that the SNR is large whenever a distinct waveform (Figs. 2b, d) is used for the correlation. Conversely, the SNR is small for the cross-correlation with wavelet c (Fig. 2c). This is expected and is caused by the large resemblance of the wavelet *c* with the waveforms in the rest of the trace. Note also that the qualitative comparison of the cross-correlograms (PCC and CCGN) from Figures 1 and 2 shows the ability of PCC to further increase the SNR. The ratios of the root mean square (rms) amplitudes CCGN to PCC are 1.28, 1.25, and 1.58 for the traces from Figure 2b, c, and d. This can be interpreted as a stronger sensitivity of waveform similarity in the PCC measure.

Detection and Coherence of Closely Similar Waveforms

A more realistic application is the detection and coherence of closely similar waveforms. The waveform perturbations are usually caused by differences in the wave propagation and the presence of noise and other signals. The

different sensitivities of the coherence measures to waveform similarity cause differences in the PCC and CCGN for waveforms that are not perfectly coherent. These differences are shown in Figure 3. The traces at the top of each figure show the pilot wavelet (solid line) and the corresponding trace with the closely similar waveform (dashed line). The pilot wavelet is shown in its full length, and the other trace is continued with zero amplitudes outside the time window shown. The cross-correlations are plotted at the bottom of each figure. Zero lag is marked by the vertical dashed line. The lag time corresponds to a shift of the pilot wavelet relative to the other waveform.

Figure 3a and b demonstrate that large amplitudes within the correlation window strongly influence the CCGN measure. The CCGN from Figure 3a does not designate whether the waveforms are best aligned at a zero time lag or a positive time lag, which aligns the waveforms by their absolute maxima or absolute maximum and minimum. In other words, following this measure the pilot and the trace can be aligned in three different manners. The time lag for the alignment of the absolute maxima is marked with a black dot. Conversely, from the PCC it is obvious that the best coherence is obtained at zero time lag only. The differences between the PCC and the CCGN measure are caused by their different concepts. The CCGN measure is based on the sum of cross-multiplication products, which is strongest influenced by the largest amplitudes in the wavelets. To show this we further increased the absolute maximum of the dashed waveform from Figure 3a; the waveforms and corresponding correlograms are shown in Figure 3b. As can be seen from this figure, the CCGN now favors the alignment of the waveforms by their absolute maxima. Conversely, PCC still advocates the alignment at zero lag. However, the PCC value at zero lag decreases, which means that the waveforms become less coherent by the modification.

The strong sensitivity of the CCGN to the large amplitudes in the waveforms also has an advantage. For instance, low amplitude noise within the correlation window will have its strongest impact when PCC is used. We show an example in Figures 3c and d. The PCC measure is equally sensitive to all perturbations in the wavelet. As consequence, the coherence value at zero lag is smaller than for the CCGN (Fig. 3c). In such a situation, the chosen length of the time window of the pilot wavelet becomes important. In Figure 3d we demonstrate the results for a decreased time window. The begin and end times of the pilot wavelet are marked by the vertical bars. The PCC measure improves, but the CCGN is little affected by this modification. Further, Figure 3 shows that the PCC maxima are more peaked than the maxima of the CCGN measure. This and the importance of the choice of the correlation window support that PCC is more sensitive to waveform coherence. In other words, PCC permits discrimination between closely similar waveforms. This is an advantage for travel-time picking or the computation of objective functions.

The different determination of waveform similarity and

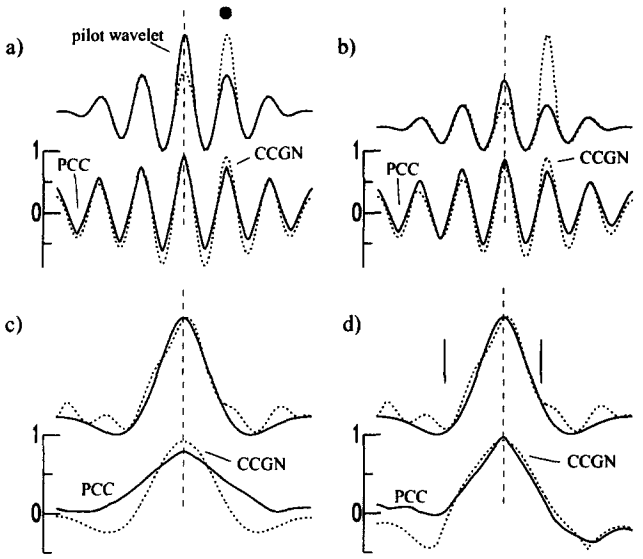

Figure 3. Comparison of PCCs and CCGNs between closely similar waveforms. (a) Top: Pilot wavelet (solid line) in its full length and trace with distorted waveform (dashed line). The distorted waveform has zero amplitudes outside the time window shown. Bottom: PCC (solid line) and CCGN (dashed line) between the pilot and the distorted signal. Zero lag is marked by the vertical dashed line and corresponds to the relative position of the waveforms at the top. (b–d) show the same as (a) for different waveforms. In (d) the pilot decreased to the time window marked by the vertical lines.

the importance of the choice of the correlation window are combined in the following example. Figure 4a shows two traces which consist of two different wave trains each. The only difference between both traces is that the last wave train (T2–T3) of the second trace is shifted by -0.2 sec. Two pilots have been extracted from the top trace using the windows T2 to T3 and T1 to T3 for correlation with the bottom trace. The resulting CCGNs and PCCs are shown in Figure 4b. The solid and dashed line style are used to distinguish the applied pilots from T2–T3 and T1–T3. As can be seen from Figure 4b, CCGN is hardly affected by the choice of the pilot. The best correlations, which are marked with a black dot, are obtained for a lag time of -0.2 sec, namely by shifting the pilot until its second wave train matches with the second wave train of the second trace. Conversely, with the PCC measure we obtain maximum correlation at 0 sec and -0.2 sec for the pilot from T1 to T3 and T2 to T3, respectively. This is due to the fact that PCC is amplitude-insensitive and consequently determines its best coherence by the maximum number of coherent samples. In other words, the zero lag alignment (dashed line) has been favored since it aligns the longest coherent wave train (T1–T2) within the pilot trace. The corresponding CCGN measure does not favor a zero lag alignment since the large amplitude wave train (T2–T3) dominates the correlation. The small amplitude parts of the correlation window lead, even in the

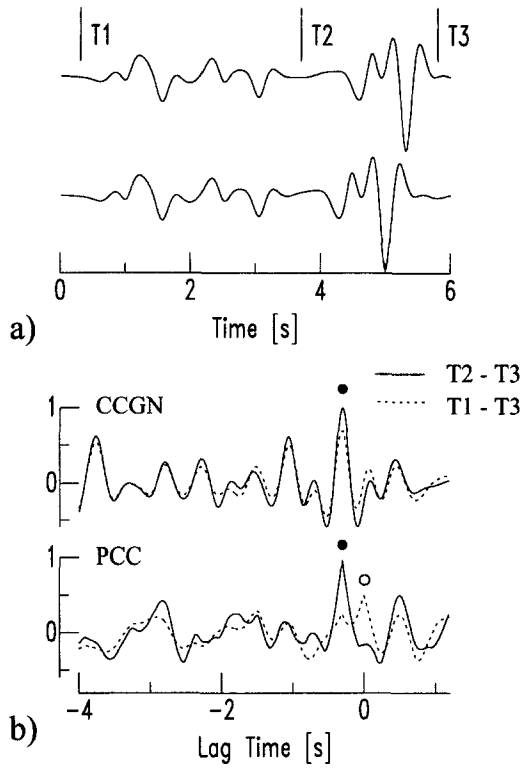

Figure 4. (a) Waveforms used for cross-correlations. Both traces consist of the same two wave trains (T1–T2 and T2–T3). The last wave train has been shifted by −0.2 sec on the bottom trace. The top trace is used to extract two different pilots (T2 to T3 and T1 to T3) that are cross-correlated with the bottom trace. (b) Cross-correlograms (top: CCGN, bottom: PCC) for the pilots T2–T3 (solid line) and T1–T3 (dashed line).

case of coherence, to small amplitude contributions that do not much affect the total correlation. This explains the large resemblance of both CCGN functions. The smaller absolute maxima of the dashed lines indicate the decreased similarity of the cross-correlated waveforms.

Significance of Different Results

So far we have presented single case studies to understand and illustrate the similarities and differences between CCGN and PCC. We considered closely coherent waveforms that have been perturbed by nondeterministic noise or in a systematic manner. Due to the different design philosophies, differences in the correlograms are observed. The type of application and the data itself determines whether these differences are significant or not, and consequently, which type of correlation should be used. Due to the variety of applications, data signal, and noise, no global statements can be made. Nevertheless, we want to reconsider an example of randomly perturbed waveforms and more systematically perturbed signals by taking into account a large number of correlations. This will give an idea about the significance of the different correlation results. In particular, we are now interested into the distribution of lag times that correspond to the best waveform alignment of closely similar waveform pairs.

Figure 5a sketches the generation of closely similar waveforms caused by a weak random perturbation. We generate a pulse function that consists of three random amplitude spikes randomly distributed within a 6 sec time window. A perturbed pulse function is produced by randomly changing the amplitudes of two spikes of the pulse function. The perturbations range from −40% to 40%. Then, both pulse functions have been band passed (0.08–0.2 Hz) to generate the finite-frequency waveforms. We use finite-length pilots of 15 sec to exclude the low amplitude tails from the correlations. The described procedure is used to randomly generate closely similar waveform pairs that will be cross-correlated. Four of the waveform pairs are shown in Figure 5b. The vertical bars mark the begin and end time of the pilots (solid lines). The numbers at the upper left and right are the lag times that correspond to the absolute maximum correlation using CCGN and PCC, respectively. A total of 5000 random waveform pairs have been generated and cross-correlated. The distribution of the lag times that belong to the best correlations are shown in Figure 5c (PCC) and 5d (CCGN). The dark gray area demonstrates the lag time distribution of the 2500 best correlations out of the 5000 performed correlations. Although we obtain different lag times for the individual cross-correlations (Figure 5b) the overall distributions resemble each other. The standard deviations of the 5000 PCC and 5000 CCGN lag times differ by about 0.2 msec, which we consider not to be significant. An increase/decrease of the pilot length by 4 sec changes the difference of the standard deviations ($\sigma_{CCGN} - \sigma_{PCC}$) to about 4.4 msec and −7.5 msec, respectively.

We repeated this experiment for other settings and obtained similar results. Consequently, it seems that PCC and CCGN are equally suited to find the best waveform alignment when nondeterministic weak perturbations cause the differences of the waveforms.

An example for a deterministic waveform perturbation is shown in Figure 6. In Figure 6a we picture the procedure used to generate the closely similar waveform pairs. Two pulse functions are generated with two random amplitude spikes at random time within a 1 s window. The first and second pulse function have been bandpassed at 1–3 Hz and 0.5–1.5 Hz, respectively. The high-frequency bandpass produces signals that are about twice as large as the low-frequency bandpass. Therefore, the second trace was multiplied by 1.5 to counteract large amplitude differences between the waveforms. Finally, the resulting traces were added after shifting the low-frequency trace by 0.2 sec and without shifting the traces to obtain the pilot and its closely similar waveform. This procedure mimics the generation of composite signals due to multipathing. In other words, the obtained signals consist of two or more distinct signals that arrive with different slowness and amplitude values at about the same time at slightly different station locations. The length of the

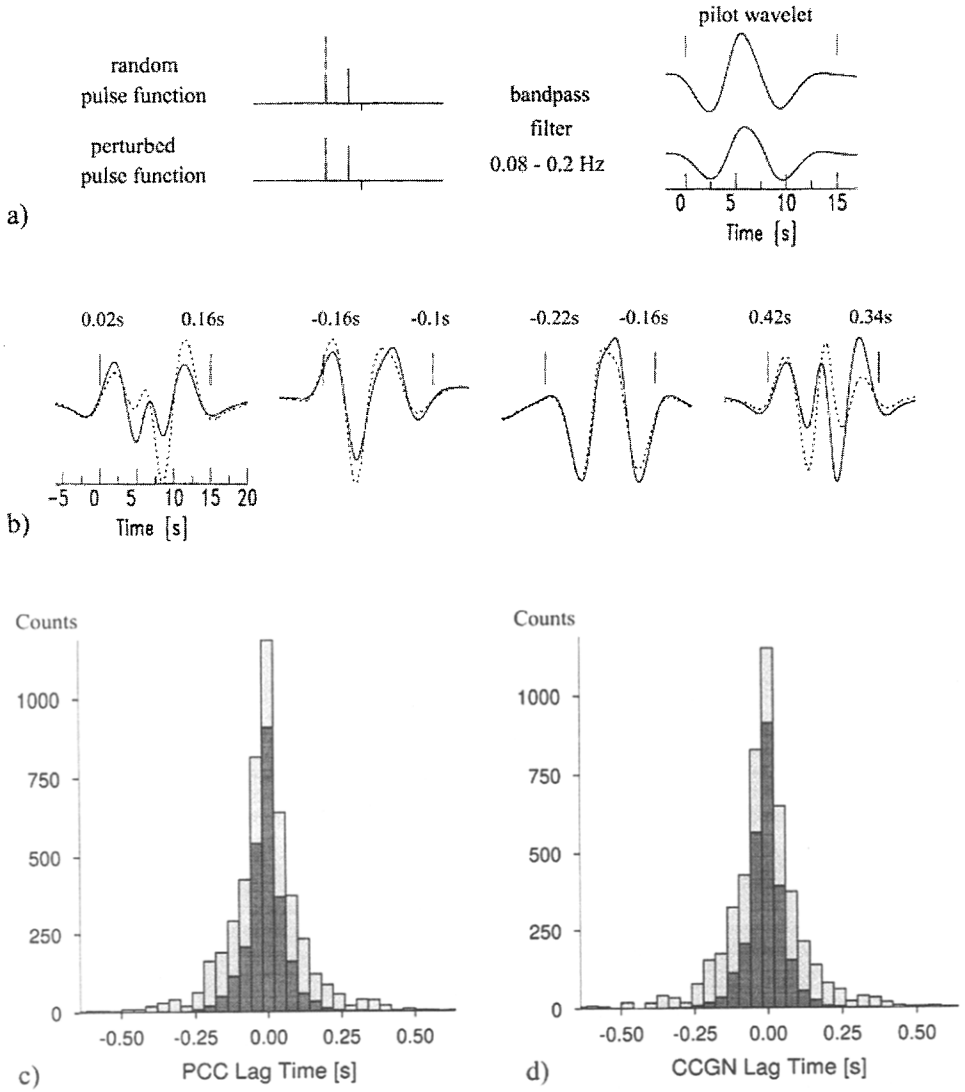

Figure 5. (a) Outline of the random generation of closely similar waveforms (see text for details). Same time scale is used for the pulse functions and finite-frequency waveforms. (b) Four examples of randomly generated pilots (solid lines) and their closely similar waveforms (dashed lines). The vertical bars mark the window (15 sec) of the pilot wavelet. The numbers at the upper left and right of each waveform pair give the lag times for the best waveform fit using CCGN and PCC, respectively. (c) and (d) The histograms show the PCC and CCGN lag time distributions of the waveform fits for 5000 randomly generated waveform pairs. The distribution of the 2500 best correlations out of the 5000 correlations is shown with the dark gray area.

pilot (solid line) is chosen to be 1.8 sec and is marked by the vertical bars in Figure 6a and b. Figure 6b shows 10 examples of waveform pairs that are generated by the described procedure. The numbers at the upper left and right mark the lag times that correspond to the best waveform fit using CCGN and PCC, respectively. Five thousand waveform pairs have been generated and correlated. The lag time distributions of the best waveform fits are presented in Figure 6c (PCC) and 6d (CCGN). The histograms in the dark gray tones show the distribution of the 2500 best correlations.

It can be seen that the distributions are significantly different. The PCC lag time distribution shows a balanced waveform alignment between both signals, that is, at -0.2 sec and 0 sec lag time. Conversely, the CCGN lag time distribution contains a clear maximum at 0 sec. This means that the waveform alignment is governed by the high frequency signal [$a(t)$ in Figure 6a], which has not been shifted in time prior to summation. On average this signal is larger than the low-frequency signal and consequently favored by the CCGN measure. A considerable amount of waveform pairs

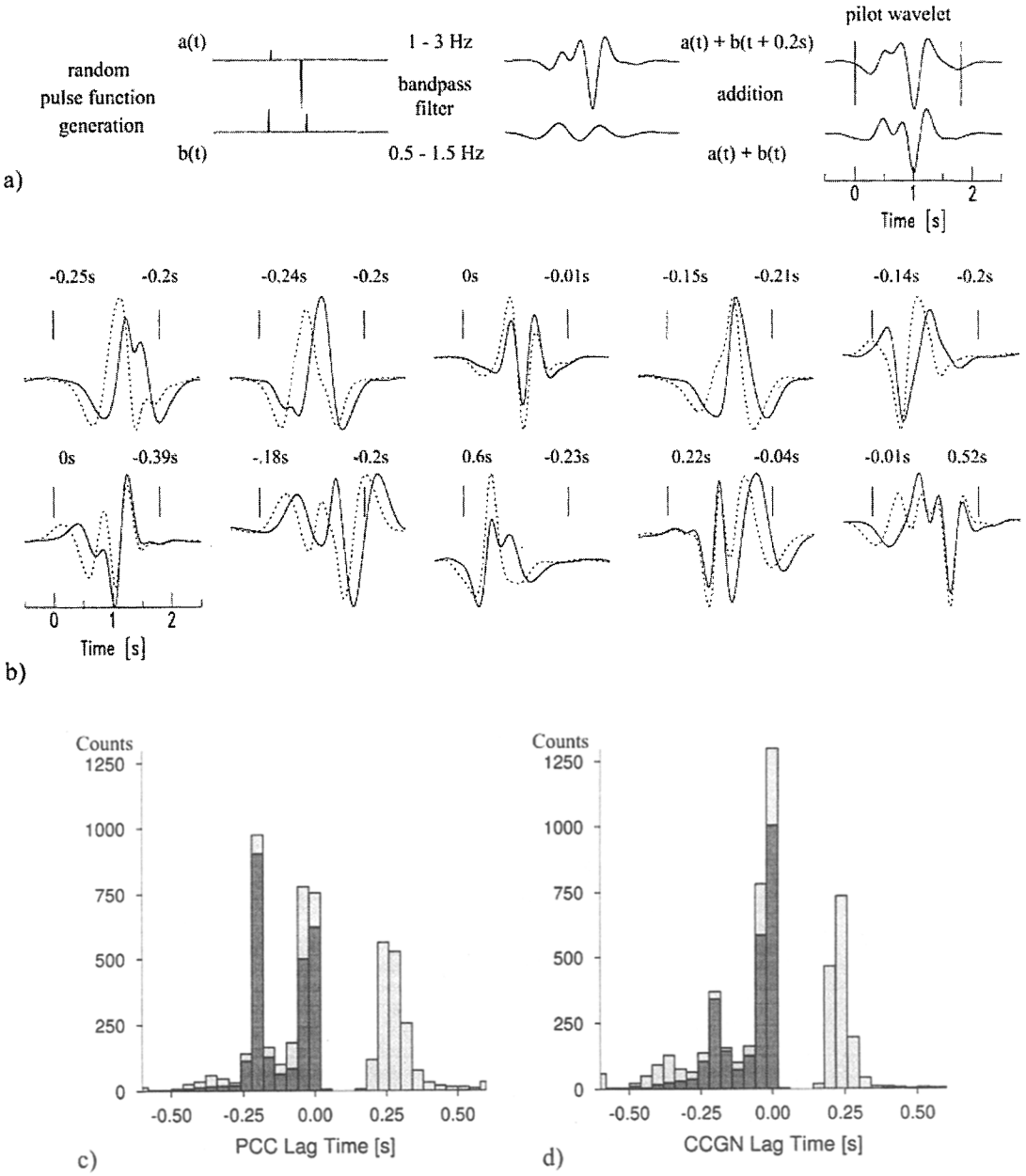

Figure 6. (a) The sketch outlines the generation of closely similar waveform pairs by the addition of two randomly generated signals. The pilot wavelet is generated by shifting the low-frequency signal by 0.2 sec prior addition. (b) Ten examples of randomly generated waveform pairs. The vertical bars mark the 1.8 sec window of the pilot (solid line). The numbers at the upper left and right are the lag times of the best CCGN and PCC waveform fits. (c) and (d) The histograms show the lag time distributions of the best PCC and CCGN waveform fits of 5000 randomly generated waveform pairs. The dark grey area shows the distributions for the 2500 best correlations.

have been aligned with positive lag times (maximum at about 0.25 sec). In these cases, the coherence measures advocate a negative waveform correlation. If PCC is used, then these cycle skips will rapidly decrease with increasing pilot lengths. For instance, increasing the length by 0.5 sec decreases the number of cycle skips to about one fifth for PCC, while the number of cycle skips of the CCGN measure remains almost unchanged. The CCGN lag time distribution shows only minor changes, and the PCC lag time distribution contains an increased number of correctly aligned waveforms. The example from Figure 6 shows the ability of PCC to detect coherent weak amplitude features that are concealed by larger amplitude signals.

Detection of Coda Phases

In this section we apply the PCC measure to the *P*-wave coda to illustrate its ability to detect weak coda phases on single seismic recordings. We are interested to reveal *P*-to-*s* conversions on radial (R) component seismograms by the waveform similarity with the corresponding *P* phases from the vertical Z components. The data set used is from three to nine portable broadband seismograph systems that have been deployed at 21 sites across SE Brazil during the Brazilian Lithosphere Seismic Projects BLSP92 (1992–1995) and BLSP95 (1995–present). For a description of these projects and station sites see James *et al.* (1993) and Assumpção *et al.* (1997), respectively.

Here we are interested in the performance of the PCC measure and the detection of *P*-to-*s* conversions rather than a site-dependent discussion of the implications of the detected features. Our approach is simple and can be summarized by the following steps: (1) Z and R components for events at distances between 35° and 95° and body wave magnitudes larger than 4.9 were selected, and no selection criteria on the event depths were imposed because the maximum variation of the theoretical *P*-to-*s* lag times is about 0.5 sec (almost all events were from shallow depths); (2) the first onsets on the Z components were picked, bandpassed (0.02–0.2 Hz), the data with an SNR of 6 or better were selected, and the reference phases or pilots for the cross-correlations were assigned using a fixed window length of 13 sec starting at the pick onsets; (3) the cross-correlation functions between the *P* waveforms and the R components and the *P* waveforms and the Z components were computed, and a fixed window length of 13 sec was used for all the reference phases; (4) maxima of the correlograms from the R and Z components were identified, and the maxima of the correlations with the R components were saved whenever there were no correlation peaks larger than 0.2 for the corresponding Z components within a 2 sec window to help eliminate phases in the R component that were not *S* arrivals.

After the execution of this procedure, we obtained the correlation peaks of 127 R component seismograms. The 80 best PCC (black dots) and CCGN (open circles) peaks have been plotted in Figure 7a. These peaks correspond to coherence values greater than or equal to 0.64 (PCC) and 0.71 (CCGN). The dashed lines mark the theoretical arrival time curves for the *Pms, Ppms, P210s, P410s, P510s,* and *P660s* phases for a hypocenter depth of 33 km. AK135 (Kennett *et al.*, 1995) was employed as the velocity model. The *Pds*-type phases are *P* waves that were converted to an *S* wave at a discontinuity at depth *d*. Moho discontinuity is represented by *m*. A *Ppms* phase experienced a *P*-wave reflection at the Earth's surface and a reflection-conversion from the Moho discontinuity. The waveforms of these arrivals will resemble the direct *P* waveforms when no waveform distortions occur due to structural complexities and/or interferences with other signals. The low frequencies used insure that there are no waveform distortions at the relatively sharp (4–20 km) mantle discontinuities. (A plane discontinuity with velocity profile that is not homogeneous acts on the *P* waveforms as a low-pass filter with corner frequencies that increase for decreasing discontinuity thickness [Richards, 1972; Paulssen, 1988].)

It can be seen from Figure 7a that several correlation peaks are clustered around the predicted travel times. It seems that some of these peaks are only detected by PCC or CCGN. This is due to the threshold used to plot the best signals. Most of the signals are detected by both techniques; however, different coherence values were assigned by CCGN and PCC. There are also visible differences in the lag times (up to about 0.3 sec) between the CCGN and PCC.

For Figure 7b, we process differently to show the robustness of the detected signals. We use an SNR threshold of 5 and employed the frequency bands 0.02–0.2 Hz with 14 sec and 20 sec pilots, 0.02–2 Hz with 12 sec and 18 sec pilots, 0.03–0.3 Hz with 12 sec pilots, and 0.04–0.4 Hz with 16 sec pilots to obtain a common data base for the PCC peaks and CCGN peaks, respectively. Only the 800 best signals were selected from each data set. The corresponding coherence values are greater than or equal to 0.5 (PCC) and 0.57 (CCGN). The 100 best signals that have been detected at least two times with PCC (black dots) or CCGN (open circles) are plotted.

Although some of the signals from Figure 7 may have been caused by occasional coherence, especially when a simple pilot waveform was used, clear signatures can be observed from the Moho and 660-km discontinuity. At higher frequencies (not shown), *Pms* arrivals can be clearly observed due to the decreased interference with other crust reverberations. The *Ppms* and *Pms* lag times imply an average Moho depth of about 42 km, in general agreement with the results of Assumpção *et al.* (1997). The 410-km discontinuity is only intermittently observed. This does not exclude the presence of *P410s* phases but indicates that such arrivals can be less coherent. Figure 7 further shows coherent signals that are grouped along the travel-time curve for the *P510s* phase. This can be interpreted as a first hint for a possible 510-km discontinuity underneath SE Brazil. The signals with lag times from 20 sec to 40 sec could not be assigned to any prominent mantle conversions/reflections. However, a 210-km discontinuity is reported in a study by Clarke *et al.* (1995), which studied *ScS* and *sScS* reverberations for the same region. The absence of *P210s* phases may indicate that the waveforms are perturbed, which may be due to interferences with other signals or lateral heterogeneities in the vicinity of the discontinuity.

The lag times of the detected arrivals (Figure 7) are generally very robust to the different applied-correlation settings. Conversely, the PCC correlation values are sensitive to changes of the employed filter and window length whenever an incoherent signal is included or excluded. This sensitivity is caused by the equal weighting of every sample in the correlation. Therefore, a more sophisticated detection should use an individual windowing of each *P* arrival to

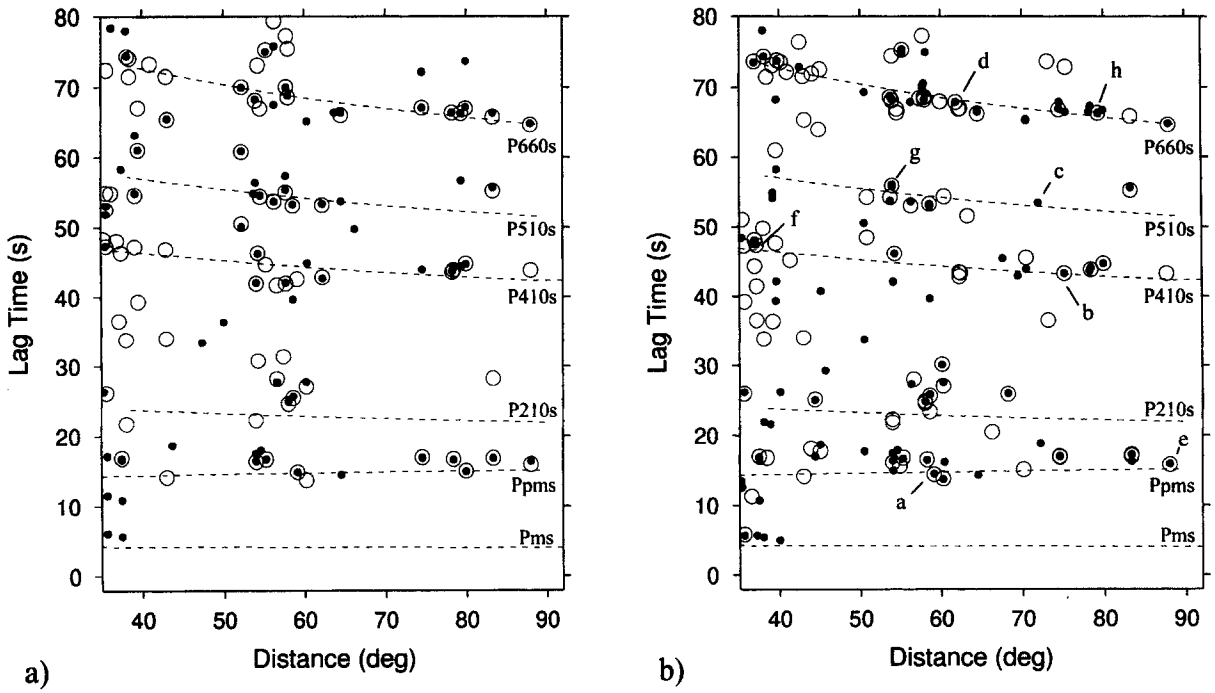

Figure 7. Cross-correlation peaks for *SV*-wave data obtained with PCC (black dots) and CCGN (open circles). Vertical axis is the time lag from the first *P* arrival. The dashed lines mark the theoretical travel time curves. (a) Plotted are the 80 best correlation peaks (PCC $\geq$ 0.64 and CCGN $\geq$ 0.71) that have been obtained by the correlation of the pilots (first 13 sec of the vertical component *P*-wave) with the corresponding R components at 0.02–0.2 Hz. (b) 100 best PCC (CCGN) peaks, which are detected at least twice using different frequency bands and pilot lengths.

improve the performance of the PCC technique. In spite of using a fixed window length for all events and stations, Figure 7 shows the ability to detect weak coda phases.

The waveforms of eight signals (*Ppms, P410s, P510s,* and *P660s* phases) are presented in Figure 8. Their corresponding correlation peaks are labeled in Figure 7b. The source parameters and station names are listed in Table 1. The conversions/reflections (solid lines) from Figure 8a–d are compared with the time-shifted pilots (dashed lines) at two frequency bands (0.02 Hz–0.2 Hz and unfiltered). In Figure 8e–h the pilots (dashed) from four other unfiltered records are compared with the detected signals on the R component and their corresponding waveforms on the Z component. Figure 8 shows that the detected signals resemble their pilots and that the correlated signals clearly dominate the R components; the lack of correlation of the pilot with the Z component is an indication of *S* arrival. The coherence of pilot and signal (Figure 8) can be observed in the unfiltered traces, which means that these examples are robust, that is, do not require special filter settings.

Discussion

We propose a new coherence functional (PCC) to evaluate quantitatively the goodness of waveform fit which can be used for signal recognition, arrival time picking, and as a misfit function. This measure is based on the similarity of instantaneous phases and computed without explicitly involving the envelopes or the amplitudes of real time series. As consequence, PCC equally weights the different amplitude portions of the waveforms within the correlation window.

The performance of PCC has been compared with the CC normalized by the geometric mean energy (CCGN). The CCGN has been employed because many other coherence functionals are based on the same principles (Neidell and Taner, 1971; Gelchinsky *et al.*, 1985; among others). We showed that CCGN is amplitude-biased and that it tends to align the waveforms by their maximum energy integral. Conversely, PCC determines the best waveform similarity by finding the largest portion of the pilot that is phase-coherent with the corresponding trace. This difference in the performance accounts for the different sensitivity to waveform variations. The small amplitude parts of the CCGN window, even in the case of coherence, have only small contributions to the total correlation. This explains why the CCGN measure remains almost unaffected when the length of the pilot is changed without including or excluding large amplitude features (see Fig. 3c and d and Fig. 4 as examples). Conversely, PCC is equally sensitive to the inclusion of small or large amplitude signals into the PCC window. This allows PCC to discriminate between closely similar waveforms. The

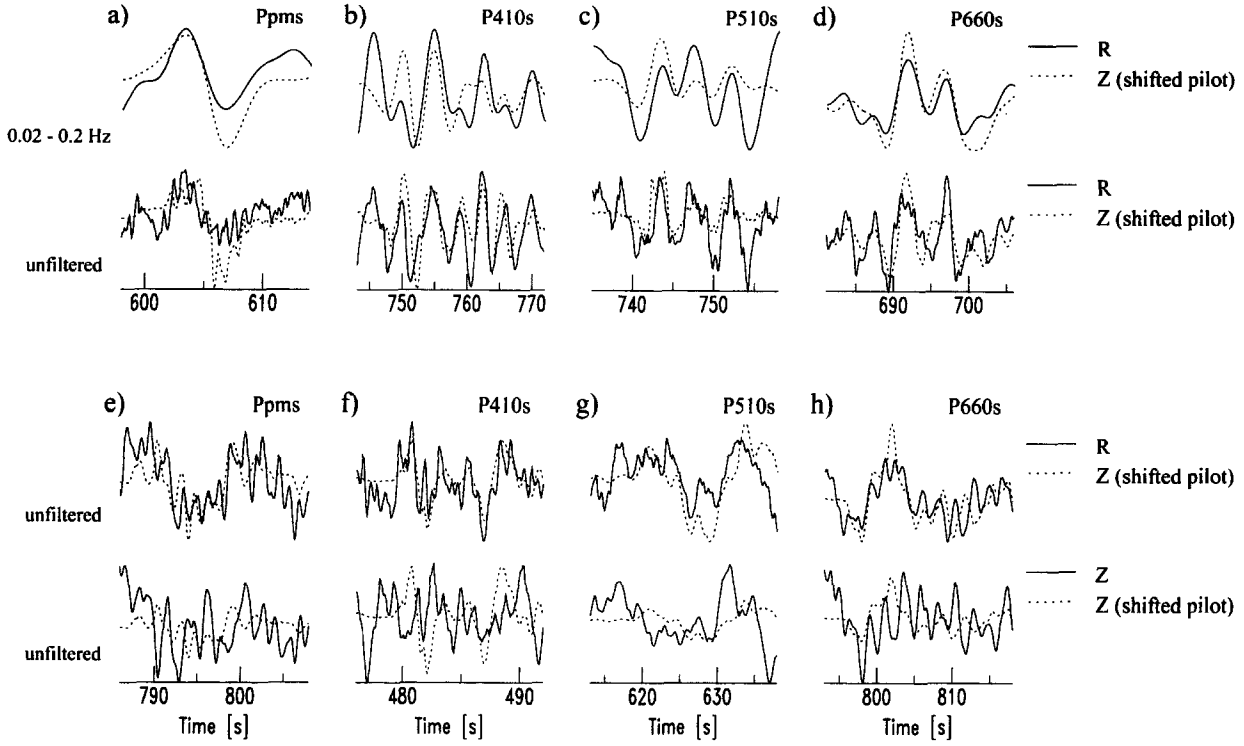

Figure 8. Waveform comparison for selected arrivals that have been detected as *P*-to-*s* reflections/conversions in the *P*-wave coda. The figure labels a–h mark the corresponding peaks in Figure 7b. Station and hypocenter information is listed in Table 1. The origin of the time axis is the event origin time. In Figures (a–d) we compare a *Ppms, P410s, P510s,* and *P660s* arrival from the R component (solid) with the time shifted pilot on the Z component (dashed) for a bandpass 0.02–0.2 Hz and unfiltered. Parts e–h compare the detected arrivals on the R and Z components (solid line) with the time shifted pilots (dashed line).

Table 1
Seismograms Used for the Waveform Comparison of *P*-to-*s* Conversions (Figure 8)[a]

Fig. 8	Year	DoY	Lon (°N)	Lat. (°E)	Depth (km)	Dist. (°)	Stat.	Fact
(a)	1994	073	−92.4	−16.0	164	59.1	CDCB	4,5
(b)	1994	320	−142.6	−56.2	10	75.1	AGVB	5,5
(c)	1993	108	−133.9	−54.0	18	71.9	RIFB	10,10
(d)	1994	185	−97.3	14.9	15	61.8	FRMB	7,5
(e)	1994	017	−118.5	34.2	18	88.0	CACB	8,8
(f)	1995	003	−56.9	−57.7	14	37.2	PPDB	6,6
(g)	1993	253	−92.6	14.7	34	54.0	AGVB	8,8
(h)	1994	043	−128.8	−10.8	15	79.3	FURB	10,10

[a]DoY stands for day of the year and Fact are the factors used to multiply the *P*-to-*s* conversions and corresponding waveforms on the Z component for the waveform comparison with the *P* arrival. The first number corresponds to the amplitude factor used for the upper traces of Figure 8.

described amplitude bias of CCGN has no effect when the waveforms are completely phase-coherent because the geometrical normalization now cancels all amplitude contributions. In reality we are mostly dealing with noisy data and should therefore be aware of possible amplitude biases whenever CCGN or similar measures are employed.

Whether PCC or CCGN is the more appropriate measure depends on the definition of the signal, the properties of the data, and the application. We suggest to apply the PCC technique whenever there are large amplitude variations in the waveforms and one seeks to measure the coherence without amplitude bias. PCC is well suited for the detection of small amplitude features that are concealed by other larger amplitude signals. For many other applications, the CCGN measure may be the better choice. A waveform alignment by the maximum energy integral can be more appropriate when the signals are strongly perturbed by noise. In this case, the large sensitivity of PCC might prohibit detection of these signals. On the other hand, PCC allows discrimination between closely similar waveforms allowing more accurate measures of the lag time of closely coherent signals. For instance, the PCCs shown in this manuscript contain narrower peaks than the CCGNs, that is, their lag times are better defined. For some applications, the differences between both measures might be insignificant. In this case the CCGN measure would be the faster method because it requires less computation operations.

In a real data example, we show the ability of PCC to detect weak *P*-to-*s* conversions/reflections in R component

seismograms by their coherence with the *P* arrival. The PCC and CCGN were used without any sophisticated processing because this might obscure the performance of the functions used. Many coherent signals were detected. A better adjustment of the pilot windows would have improved the detection with PCC. The most robust features in our data base are caused by the Moho and 660-km discontinuity. This does not mean that these are the strongest discontinuities but that the signal waveforms are less perturbed in our data set. The average Moho depth of about 42 km confirms the results by Assumpção *et al.* (1997), they obtained similar depth values using receiver functions. The *P410s* arrivals are more intermittently observed. The interferences with other signals or structural complexities such as topography (Neele and Snieder, 1992; Van der Lee *et al.,* 1994) can decrease the similarity with the *P* waveform and therefore decrease the seismic visibility. Structural complexities are indeed expected due to the presence of a fossil plume conduit in the upper mantle in SE Brazil revealed in a tomography study by VanDecar *et al.* (1995). Consequentially, parts of the upper mantle are warmer than the average and the thickness, topography, and depth of the discontinuities will vary in response to the temperature variations (Helffrich and Bina, 1994). The 410-km and 660-km discontinuities were also observed using *ScS* and *sScS* reverberations by Clarke *et al.,* (1995). They further report the observation of a 210-km discontinuity that can not be confirmed from Figure 7.

Our results show coherent phases with travel times and slowness values that correspond to *P*-to-*s* conversions from the 510-km discontinuity. A more detailed study is required to investigate the properties of these conversions and their implications for the transition at 510-km depth. The 510-km discontinuity has been intermittently observed as reported by Shearer (1990), Revenaugh and Jordan (1991), and Mechie *et al.,* (1993), among others. The origin of this discontinuity is still unknown (Stixrude, 1997).

Conclusions

We have developed a sensitive coherence measure (PCC) that is useful for signal recognition, arrival time picking, and as an objective or misfit function for waveform comparisons. The PCC is amplitude-unbiased in contrast to CC and CCGN. The CCGN tends to align the waveforms by their maximum energy integral, and PCC determines the best waveform similarity by finding the largest portion of the pilot that is phase-coherent with the corresponding trace.

The significance of the different performances of CCGN and PCC and the choice of the proper technique depend on the application, data, and signal definition. We conclude that PCC is the better measure to detect weak signals that are concealed in other larger amplitude signals. Due to its large sensitivity to small amplitude variations PCC enables a better discrimination between closely similar waveforms. This can be advantageous for waveform fitting and stripping techniques. The larger sensitivity can also permit a more accurate determination of travel time. Strongly perturbed waveforms might be better detected with CCGN since it is less sensitive to waveform perturbations and based on the maximum energy integral.

We showed the ability of PCC to detect weak upper mantle conversions using a data set of seismic broadband recordings from SE Brazil. With this test, we present confirming evidence for seismic discontinuities at about 42 km, 410 km, and 660 km depth. Further, hints of a 510-km discontinuity could be observed. A more detailed study on the seismic visibility and structural implications of the detected phases is required, but this was not the objective of this manuscript.

Acknowledgments

The author would like to thank Marcelo Assumpção for many helpful discussions. The Associate Editor W.R. Walter and the Referees F. Neele and P. Shearer are acknowledged for their reviews. The data are from the Brazilian Lithosphere Seismic Project that was started as a joint project from the Carnegie Institution of Washington and the Institute of Astronomy and Geophysics (IAG) in São Paulo, and was continued by the IAG. The author is grateful to all the researchers and technicians who contributed to the data set. Plots were done with the Seismic Analysis Code (SAC), which was provided by Lawrence Livermore National Laboratory of the University of California, and Generic Mapping Tools (GMT) by Wessel and Smith (1991). This work is supported by the FAPESP (Fundação de Amparo à Pesquisa do Estado de São Paulo).

References

Assumpção, M., D. James, and J. A. Snoke (1997). Crustal thickness in SE Brazilian shield with receiver function: isostatic compensation by density variations in the lithospheric mantle? *5th congresso international da sociedade brasileira de geofísica,* São Paulo, September 28–October 2, 1997, 895–897.

Bracewell, R. N. (1965). The Fourier Transform and its Applications, Mcgraw-Hill, New York, 268–271.

Clarke, T. J., P. G. Silver, Y. L. Yeh, D. J. James, T. C. Wallace, and S. L. Beck (1995). Close in *ScS* and *sScS* reverberations from the 9 June 1994 Bolivian earthquake, *Geophys. Res. Lett.* **22,** 2313–2316.

Diogo, L. A. (1995). Otimização simplificada para inversão sísmica cinemática, *Ph.D. Thesis* Universidade Federal da Bahia (in Portugese).

Gelchinsky, B., E. Landa, and V. Shtivelman (1985). Algorithms of phase and group correlation, *Geophys.* **50,** 596–608.

Helffrich, G. R., and C. R. Bina (1994). Frequency dependence of the visibility and depth of mantle seismic discontinuities, *Geophys. Res. Lett.* **21,** 2613–2616.

James, D. E., M. Assumpção, J. A. Snoke, L. C. Ribotta, and R. Kuehnel (1993). Seismic studies of continental lithosphere beneath SE Brazil, *An. Acad. bras. Ci.* **65,** 227–250.

Kanasewich, E. R., C. D. Hemmings and T. Alpaslan (1973). N-th root stack nonlinear multichannel filter, *Geophys.* **38,** 327–338.

Kennett, B. L. N., E. R. Engdahl, and R. Buland (1995). Constraints on seismic velocities in the Earth from travel times, *Geophys. J. Int.* **122,** 108–124.

Krüger, F., M. Weber, F. Scherbaum, and J. Schlittenhardt (1993). Double beam analysis of anomalies in the core-mantle boundary region, *Geophys. Res. Lett.* **20,** 1475–1478.

Mao W., and D. Gubbins (1995). Simultaneous determination of time delays and stacking weights in seismic array beamforming, *Geophysics* **60,** 491–502.

Mechie, J., A. V. Egorkin, K. Fuchs, T. Ryberg, L. Solodilov, and F. Wen-

zel (1993). *P*-wave mantle velocity structure beneath northern Eurasia from long-range recordings along the profile Quartz., *Phys. Earth Planet. Interiors* **79,** 269–286.

Muirhead, K. J. (1968). Eliminating false alarms when detecting seismic events automatically, *Nature* **217,** 533–534.

Neele, F., and R. Snieder (1991). Are long-period body wave coda caused by lateral inhomogeneity?, *Geophys. J. Int.* **107,** 131–153.

Neele, F., and R. Snieder (1992). Topography of the 400 km discontinuity from observations of long period P400P phases, *Geophys. J. Int.* **109,** 670–682.

Neidell, N. S., and M. T. Taner (1971). Semblance and other coherency measures for multichannel data, *Geophys.* **36,** 482–497.

Paulssen, H. (1988). Evidence for a sharp 670-km discontinuity as inferred from *P* to *S* converted waves, *J. Geophys. Res.* **93,** 10489–10500.

Revenaugh, J., and T. H. Jordan (1991). Mantle layering from *ScS* Reverberations, 2, The transition zone, *J. Geophys. Res.* **96,** 19763–19800.

Richards, P. G. (1972). Seismic waves reflected from velocity gradient anomalies within the Earth upper mantle, *Z. Geophys.* **38,** 517–527.

Schimmel M., and H. Paulssen (1997). Noise reduction and detection of weak, coherent signals through phase weighted stacks, *Geophys. J. Int.* **130,** 497–505.

Sen, M. K., and P. L. Stoffa (1991). Nonlinear one-dimensional seismic waveform inversion using simulated annealing, *Geophys.,* **56,** 1624–1638.

Shearer, P. M. (1990). Seismic imaging of upper-mantle structure with new evidence for a 520-km discontinuity, *Nature* **344,** 121–126.

Stixrude, L. (1997). Structure and sharpness of phase transitions and mantle discontinuities, *J. Geophys. Res.* **102,** 14835–14852.

Taner, M. T., F. Koehler, and R. E. Sheriff (1979). Complex seismic trace analysis, *Geophys.* **44,** 1041–1063.

VanDecar, J. C., and R. S. Crosson (1990). Determination of teleseismic relative phase arrival times using multi-channel cross-correlation and least squares, *Bull. Seismol. Soc. Am.* **80,** 150–169.

VanDecar, J. C., D. E. James, and M. Assumpçãc (1995). Seismic evidence for a fossil plume beneath South America and implications for plate driving forces, *Nature* **378,** 25–31.

Van der Lee, S., H. Paulssen, and G. Nolet (1994). Variability of *P660s* phases as a consequence of topography of the 660 km discontinuity, *Phys. Earth Planet. Interiors* **86,** 147–164.

Wessel, P., and W. H. F. Smith (1991). Free software helps map and display data, *EOS* **72,** 441, 445–446.

Zürn, W., and P. A. Rydelek (1994). Revisiting the phasor-walkout method for detailed investigation of harmonic signals in time series, *Surv. Geophys* **15,** 409–431.

Instituto Astronômico e Geofísico
Universidade de São Paulo
Rua do Matão 1226
05508-900 São Paulo, SP, Brazil
E-mail: *martin@iag.usp.br*

Manuscript received 27 October 1998.